Journal of the Korean Society of Surveying, Geodesy, Photogrammetry and Cartography
Vol. 34, No. 2, 143-151, 2016
http://dx.doi.org/10.7848/ksgpc.2016.34.2.143

ISSN 1598-4850(Print)
ISSN 2288-260X(Online)
Original article

Detection of Seabed Rock Using Airborne Bathymetric Lidar and Hyperspectral Data in the East Sea Coastal Area

Shin, Myoung Sig[1] · Shin, Jung Il[2] · Park, In Sun[3] · Suh, Yong Cheol[4]

Abstract

The distribution of seabed rock in the coastal area is relevant to navigation safety and development of ocean resources where it is an essential hydrographic measurement. Currently, the distribution of seabed rock relies on interpretations of water depth data or point based bottom materials survey methods, which have low efficiency. This study uses the airborne bathymetric Lidar data and the hyperspectral image to detect seabed rock in the coastal area of the East Sea. Airborne bathymetric Lidar data detected seabed rocks with texture information that provided 88% accuracy and 24% commission error. Using the airborne hyperspectral image, a classification result of rock and sand gave 79% accuracy, 11% commission error and 7% omission error. The texture data and hyperspectral image were fused to overcome the limitations of individual data. The classification result using fused data showed an improved result with 96% accuracy, 6% commission error and 1% omission error.

Keywords : Seabed rock, Detection, Bathymetric Lidar, Hyperspectral Image

1. Introduction

The coast is an interactive place among the land, ocean, and atmosphere which is influenced greatly by climate change and development. In Korea, around 34% of the cities are close to the coast, and around 60% of the power plants and more than half of the industrial complexes are located on the coast. However, information about the coastal area of Korea is still insufficient (Oh *et al.,* 2004).

Investigation of seabed material has high importance because it is associated with the development and preservation of the ocean, navigation safety, and military actions. The traditional survey methods for seabed material can be divided into two types, scuba diving and surveying with a vessel. Scuba diving is the most accurate method, but it is inefficient in relation to the area covered and time. Surveying with a vessel sets sample points with constant distance. It is more efficient compared to scuba diving in the relation to area coverage and time. However, the point based survey with a vessel has a low density due to the time and cost, and areas may be missed due to the limitation of vessel access. At present, there is not enough precise data about how the seabed material of Korea's coast is distributed spatially.

Effective measurement and mapping technologies have been developed recently using remote sensing sensors. In a hydrographic survey, researchers are able to measure water

Received 2016. 03. 30, Revised 2016. 04. 14, Accepted 2016. 04. 29
1) Member, Korea Hydrographic and Oceanographic Agency (E-mail: shin1536@korea.kr)
2) Research Institute, Geostory Inc. (E-mail: jishin@geostory.co.kr)
3) Korea Hydrographic and Oceanographic Agency (E-mail: noripis@korea.kr)
4) Corresponding Author, Member, Dept. of Civil Engineering, Pukyung National University (E-mail: suh@pknu.ac.kr)

This is an Open Access article distributed under the terms of the Creative Commons Attribution Non-Commercial License (http://creativecommons.org/licenses/by-nc/3.0) which permits unrestricted non-commercial use, distribution, and reproduction in any medium, provided the original work is properly cited.

depth, coast line, and seabed topography using airborne bathymetric Lidar (Seo and Kim, 2008; Zavalas *et al*., 2014). There is a case using backscattered intensity acquired from the Lidar to detect the seabed rock (Collins *et al*., 2007). Some studies used the hyperspectral image to investigate seabed material and seaweed distribution in the intertidal zone, and types of land-cover on the coastal land area (Choi, 2014; Kim, 2014; NOAA Coastal Services Center, 2010). Other studies reported the distribution of coral reef and/or the material of the seabed present in shallow waters below 10m depth (Kim *et al*., 2013; Mishra *et al*., 2007; Ciraolo *et al*., 2006; Tamir and Arnon, 2015). However, these studies were made on a shallow and gentle seabed and did not consider the variation of spectral reflectance due to the water depth.

In Korea, airborne Lidar and hyperspectral sensors have been introduced recently where there is inadequate application of the technology, but most studies are focused on the land. Thus, there is a need to develop hydrographic surveys and investigative technologies using hyperspectral image and bathymetric Lidar data on ocean seabeds. Also, for studying seabeds with optical images, there is a need for technology to correct the variation of spectral reflectance with water depth. When the seabed slope is steep as in the East Sea, the need for corrective technology becomes greater.

This study attempts to detect seabed rock of the East Sea using airborne hyperspectral image and bathymetric Lidar data. To increase the accuracy, fused data that integrate the hyperspectral image and the seabed topographic (texture) data are suggested for detecting seabed rock.

2. Study Area and Data

The study area is the coast from Sacheonjin Port to Gyeongpo Beach in Gangneung-si, Gangwon-do. The water in this area is comparatively clear, and the seabed material is composed of sand and rock. The water depth is from 0m to 20m, and the rock is distributed at the top (Sacheonjin Port north side), middle (Sacheon Beach), and bottom (Gyeongpo Beach) parts of study area.

The airborne bathymetric Lidar data used in this study was acquired in September of 2013 with the CZMIL (Coastal Zone Mapping Imaging LiDAR) sensor of Optech Inc. in Canada. The flight altitude was 400m, and the laser scanning type was circular. The laser scanning rate was 10 kHz with 16.38 points per 5m x 5m area. The airborne bathymetric Lidar data was preprocessed in the order of GPS/INS data process, laser data process, and topographic data classification (noise removal). Then the point cloud data was converted to raster format such as DEM (digital elevation model) using the cubic convolution interpolation method. Here, the resolution of the raster data had 1m which was the same resolution as the hyperspectral image. Fig. 1(a) shows the CZMIL airborne bathymetric Lidar data that was interpolated to the raster format. In this figure,

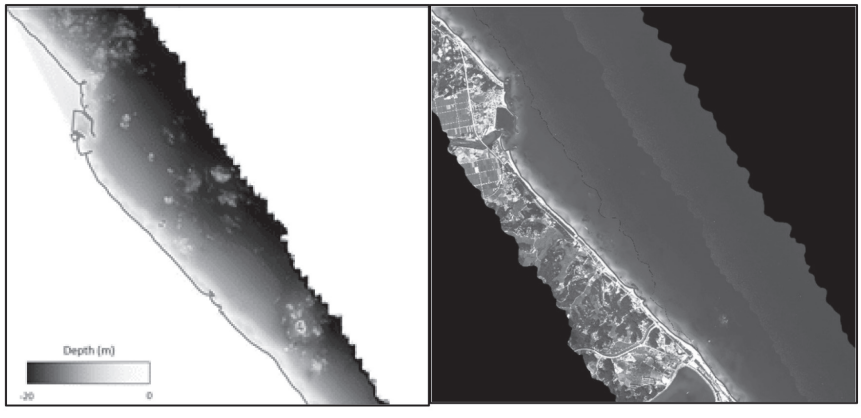

(a) (b)

Fig. 1. (a) Airborne bathymetric Lidar (CZMIL) data and (b) Hyperspectral image (CASI-1500), where red line is shore line

the shore line is indicated by the red line. The hyperspectral image was acquired in October of 2013 with the CASI-1500 sensor of Canada's ITRES. The flight altitude was 2000m, the wavelength range was 380-1050nm, the number of band was 48, and the spatial resolution was 1m. The hyperspectral image was preprocessed in two steps. The first step was a general preprocessing that included radiometric correction, atmospheric correction, and geometric correction. The second step was additional preprocessing to extract signals from the seabed which estimated the water reflectance (removal of water surface reflection) and water column correction. The additional preprocessing is explained in Chapter 4. Fig. 1 (b) shows the hyperspectral image that was preprocessed from radiometric to geometric correction.

Validation samples were collected with visual interpretation of both hyperspectral image and Lidar data. For visual interpretation of seabed material, a field survey dataset from a survey by Korea Hydrographic and Oceanographic Administration in 2015 was used as a reference. Validation samples are composed of 160 points where 80 are rock points and 80 are sand points. Fig. 2 shows the distribution of the validation samples where red and yellow refer to rock and sand, respectively.

3. Seabed Rock Detection using Bathymetric Lidar

When looking at the seabed topography, generally the rock has a rough texture compared to other materials such as mudflat or sand. Thus, when the seabed contained rock, there seemed to be a high variation in the water depth. When the water depth is expressed as a brightness value, rocky areas display uneven brightness in the texture perspective. The statistical value within the kernel or moving window was generally used to acquire the texture information. First order statistical operators include the maximum-minimum (range), average, variance, standard deviation, and entropy (Jensen, 2005).

This study applied the maximum-minimum operator for the water depth from bathymetric Lidar data to convert it to texture data. Here, the size of the moving window was applied diversely as 3 x 3, 7 x 7, and 9 x 9, and the optimum window size was decided as 7 x 7. Thus, the converted texture data showed a difference of minimum water depth and maximum water depth appearing within the space of 7m x 7m surrounding each pixel.

To detect the seabed rock, a threshold value of 0.5m was applied to the texture data. This was because the CZMIL sensor had a water depth maximum measurement error of 0.4m at 30m depth. When the difference in the water depth (maximum-minimum) was bigger than 0.5m, it was judged to be a rock. This is because the study area was shallower than 20m in depth.

Fig. 3 shows the seabed rock detection result. When visually compared with the water depth data of Fig. 1 (a), the distribution of the rock matches. However, when zooming in

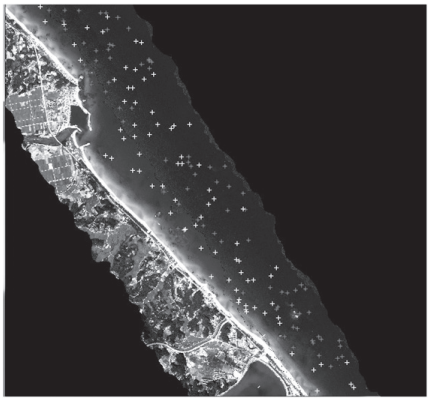

Fig. 2. Location of validation samples with eye interpretation (red: rock, yellow: sand)

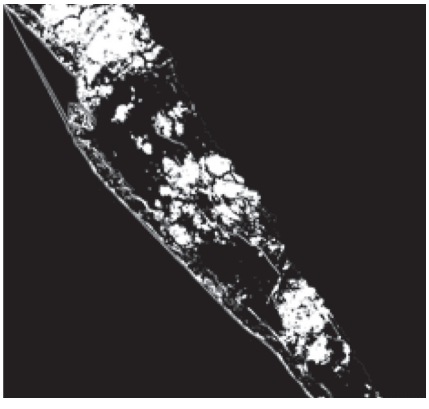

Fig. 3. Seabed rock detection result using bathy metric Lidar data

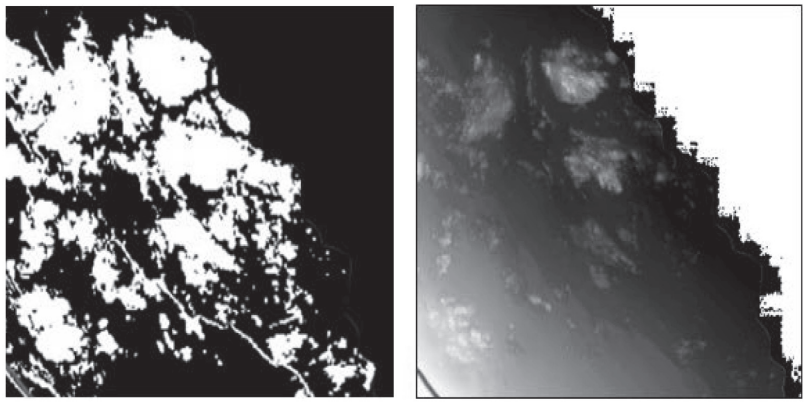

(a) (b)

Fig. 4. (a) Seabed rock detection result and (b) Bathymetric Lidar data

on some of the areas such as in Fig. 4, the detected boundary of rock is located outside the area compared to the boundary shown visually in the water depth data. This indicates over-detection. This might be caused by a blur effect which is a characteristic of the method using a moving window. The blur effect increases when the window size is large, such as a low-pass filter. On the other hand, when making the window size smaller, rock is not detected (omission error) in an area with a small variation of water depth even though rock is actually present.

To analyze the accuracy of the detection result, it was compared with 160 validation samples (Table 1). Overall, 141 points among the 160 validation points corresponded to the detection result, indicating 88% accuracy. In the case of the rock, 80 validation points were detected as rock, indicating 100% detection rate. Although 19 sandy points were detected as rocks among 80 validation points, giving 24% commission error, the explanation for the error are the characteristics of the texture operator with the moving window as mentioned above. Thus, the accuracy of the detection method using texture information needs improvement.

Table 1. Accuracy of seabed rock detection result using bathymetric Lidar data

Detection \ Reference	Rock	Sand	Total
Rock	80	19	99
Sand	0	61	61
Total	80	80	160
Detection accuracy = (80+61)/160 = 88%			

4. Seabed Rock Detection using the Hyperspectral Image

4.1 Correction for water surface reflection and water column absorption effects

The sensor records the electro-magnetic (EM) energy that is reflected or scattered from the atmosphere, water surface, water column and seabed. Thus, to estimate the signal derived only from the seabed, there must be a correction for the components of the signal (EM energy) that are derived from the atmosphere, water surface, and water column. Atmospheric correction was already included in the general preprocessing procedure of Chapter 2. Correction for the water surface reflectance requires estimating the signal component that arises from reflection of the water surface. In this study, the method of Hedley (2005) was used to estimate the reflected energy from the water surface. The method assumes that the reflectance of water is 0 or a minimum value in the near-infrared wavelength. Fig. 5 shows the comparison of the image before and after correction for water surface reflection.

Water column correction normalizes the variation of seabed reflectance by water depth. EM energy is absorbed by the water column during transmission to the seabed and

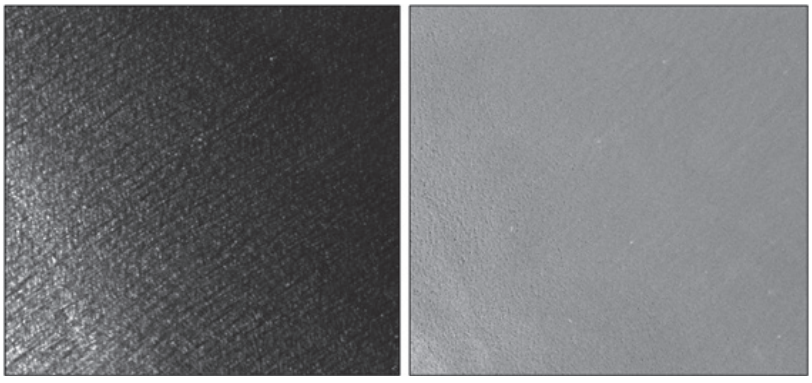

(a) (b)

Fig. 5. Hyperspectral Image (a) before water surface reflection correction and (b) after water surface reflection correction

can vary according to water quality. However, this research assumed that the water quality is constant in the narrow study area and therefore disregarded the variation in the reflectance by water quality. Lyzenga (1978) suggested Eq. (1) for the relationship of water reflectance and bottom albedo based on Beer's law.

$$R_W = (A_d - R_\infty)\exp(-gz) + R_\infty \quad (1)$$

where R_W is water reflectance, z is depth, A_d is bottom albedo, g is diffuse attenuation coefficient, and R_∞ is water reflectance at very deep water.

According to Eq. (1), the reflectance observed at the water surface (just below the surface) is the sum of the reflectance of seabed and water column which is reduced exponentially by the water depth. Thus, to estimate EM energy reflected from the seabed, the water column absorption must be normalized in relation to water depth. In this study, the water column absorption effect was corrected for the water reflectance of the hyperspectral image with 1m depth interval. Then a regression model was developed which showed the exponential relationship between water depth and water reflectance for the same seabed material. Finally, the regression model was inversely transformed into a logarithmic model for water column correction which was applied to whole image. Fig. 6 (a) shows the hyperspectral image corrected for the water column absorption effect.

4.2 Detection using the hyperspectral image

For the training sample on seabed rock detection using the hyperspectral image, pixels of target (rock) and background (sand) were collected from the pixels of the image itself. Here, the number of training samples were 100 (50 rocks, 50 sand) where the location was clear in the 1:5000 chart. The hyperspectral image was classified to rock and sand using a supervised classifier and collected training samples. This study consistently used a maximum likelihood (MLH) classifier for the hyperspectral image and fused data as is explained in Chapter 5.

Fig. 6 (b) shows the classification result using the hyperspectral image of Fig. 6 (a). When visually comparing the classification result with the hyperspectral image, the classification result matches the distribution of rock at the top, middle and bottom of the image. However, there are a lot of omission and commission errors. Some rocks were not detected due to weak signals (uncertain reflectance). Some sand in shallow areas was detected as rock. Especially, the sand of the Sacheon Beach was detected as rock. There are three possible reasons for this kind of error. First is the correction error of the hyperspectral image that might be included in correction procedures such as atmospheric correction, water surface reflectance removal and water column correction. Second is the natural variation in the reflectance from properties of seabed and water columns. Third is the environmental signal distortion such as the wave (breaker) and the shadow that occurs during image acquisition.

Table 2 shows the detection accuracy of the hyperspectral image. The overall accuracy is 79% where 126 points are matched among 160 validation samples. When analyzing the detection ratio in detail, 59 rocks are detected among 80 rocks in the validation samples, giving a 74% detection rate and a 26% omission error. Also, a commission error, where the sand is detected as rock, occurred in 13 points among the 80 sand points giving a 16% commission error.

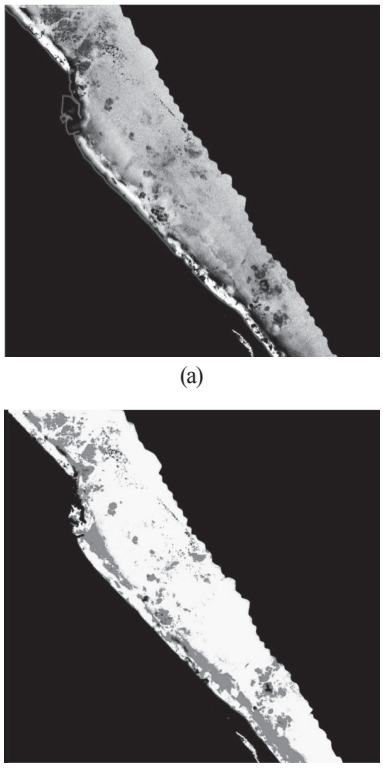

(a)

(b)

Fig. 6. (a) Water column corrected hyperspectral image and (b) MLH classification result (red is rock and yellow is sand)

Table 2. Accuracy of seabed rock detection result using hyperspectral image

Detection \ Reference	Rock	Sand	Total
Rock	59	13	72
Sand	21	67	88
Total	80	80	160
Detection accuracy = (59+67)/160 = 79%			

5. Data Fusion and Seabed Rock Detection

5.1 Fusion of hyperspectral image and texture data

Hyperspectral image and bathymetric Lidar data have advantages and disadvantages arising from the characteristics of each sensor. The hyperspectral image can estimate boundaries of seabed materials accurately using spectral reflectance, although it includes uncertainty and variation by depth, seabed properties, water quality, and imaging environments (Hedley, 2013). Bathymetric Lidar can provide depth or topographic information although it is limited with respect to spectral information for classifying seabed material (Pittman *et al*., 2013). Data fusion is a method to increase the accuracy of seabed mapping (Wozencraft and

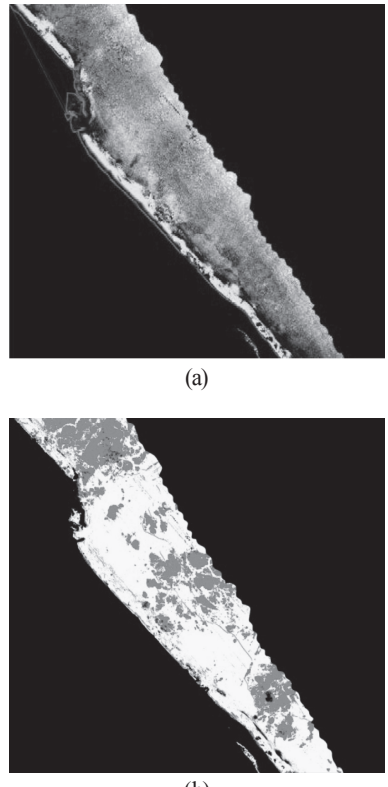

(a)

(b)

Fig. 7. (a) Color composition of fused image using hyperspectral image and texture data (R: texture, G: 632nm, B: 546nm) and (b) MLH classification result (red is rock and yellow is sand)

Park, 2013). This study attempted fusion of texture data and the hyperspectral image to overcome the uncertainty from water depth in the hyperspectral image and the limitation of spectral information in Lidar data. The texture data was added as a band in the hyperspectral image, that had 49 bands consisting of 48 spectral bands and 1 texture band. Fig. 7(a) shows a color composite of fused data (R: texture, G: 632nm, B: 546nm) where the seabed rocks are shown in red and the sand is shown as blue and green.

5.2 Detection using fused data

The maximum likelihood (MLH) classifier was used to detect seabed rock using fused data which was the same method as used for the hyperspectral image. Supervised classifiers are widely used to classify hyperspectral images. These classifiers include spectral angle mapper (SAM), support vector machine (SVM), and maximum likelihood (MLH). Previous studies employed the most widely used MLH classifier on the seabed mapping with integrated data of Lidar and hyperspectral image (Ciraolo *et al*., 2006; Wozencraft and Park, 2013). The fused data has a different signal range or different characteristics between spectral bands and a texture band. This might be a reason for limiting the use of a classifier based on spectral characteristics. The MLH classifier can consider statistical characteristics of spectral and texture information at the same time. Additionally, some studies reported better or similar accuracy of MLH than classifiers such as SAM and SVM when the training sample is adequate (Yang *et al*., 2012; Shafri *et al*., 2007). Rock and sand were classified by applying the MLH classifier to fused data. Then, only rock was extracted from the classified result for its final identification.

Fig. 7 (b) shows the classification result using the fused data of Fig. 7 (a). When visually comparing the classification result with the fused data, the classification result shows a matched and accurate boundary between rock and sand. However, some commission errors still exist, such as noise that is distributed in the very shallow area close to the shore line. Table 3 shows the accuracy of the detection results using fused data. The overall accuracy is 96% with 154 correspondent points among 160 points. In the case of rock, 79 points were detected among 80 validation samples which give a 99% detection rate, 1% omission error and 6% commission error.

Table 3. Accuracy of seabed rock detection result using fused data

Detection \ Reference	Rock	Sand	Total
Rock	79	5	84
Sand	1	75	76
Total	80	80	160
Detection accuracy = (79+75)/160 = 96%			

Fig. 8 comparing the detection results for seabed rock shows that the detection result using fused data gives a clearer boundary and fewer errors than detection results using texture data or the hyperspectral image separately.

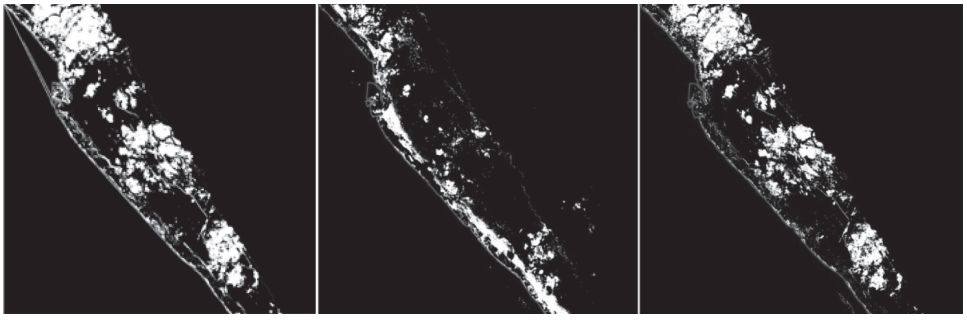

(a) (b) (c)

Fig. 8. Seabed rock detection results using (a) texture of Lidar data, (b) hyperspectral image and (c) fused data

Table 4. Comparison of accuracies among texture (Lidar), hyperspectral image and fused data

	Texture (Lidar)	Hyperspectral	Fused data
Overall accuracy	88%	79%	96%
Omission error	0%	26%	1%
Commission error	24%	16%	6%

Table 4 compares accuracies among texture from Lidar, hyperspectral image and fused data. Overall accuracy of fused data is 17%p and 8%p higher than the detection results of hyperspectral image and bathymetric Lidar data, respectively. Omission error of fused data is 25%p lower than that of hyperspectral image. Commission error of fused data is 18%p and 10%p lower than that of texture data and hyperspectral image, respectively. Therefore, the fused data provides an improved detection result and higher accuracy than the individual data sets.

6. Conclusion

This study attempted to suggest an efficient and accurate method for investigating rock distribution in coastal seabed using airborne remote sensing data. For this, texture data from bathymetric Lidar data and hyperspectral image was used individually to find out the limits and possibilities of their use. Then, the two datasets were fused to increase detection accuracy. When compared with the results using individual data, fused data had 8%p and 17%p higher overall accuracy than Lidar and hyperspectral image data, respectively. Additionally, commission error was decreased 10-18%p and omission error is decreased 25%p. Therefore, for seabed rock detection, it is better to use the fused data than individual hyperspectral image and bathymetric Lidar data.

There is a need for future studies in three different subject areas. First is the need to increase the detection accuracy. Various false alarms were found with visual interpretation although numerically 96% accuracy was obtained. Second, there is a need to subdivide the classes of materials such as the sand, gravel, and mud along with the rock. Third, additional study is needed for the expansion of the geographic region. Because the Korean Peninsula is surrounded by three seas, and the characteristics of each sea are diverse. Therefore, there is a need for additional studies which take into account these limitations and characteristics.

References

Choi, H. (2014), *A Study on Seacoast Land Cover Classification from Hyperspectral Images*, Master`s thesis, Kyonggi University, Suwon, Korea, 32p.

Ciraolo, G., Cox, E., La Loggia, G., and Maltese, A. (2006), The classification of submerged vegetation using hyperspectral MIVIS data, *Annals of Geophysics*, Vol. 49, No. 1, pp. 287-294.

Collins, B., Penley, M., and Monteys, X. (2007), Lidar seabed classification: New process for generation of seabed classes, *Hydro International*, Netherland, http://www.hydro-international.com/articles (last date accessed: 22 March 2016).

Hedley, J. D. (2013), Hyperspectral applications, In: Goodman, J. A., Purkis, S. J. and Phinn, S. R. (eds.), *Coral Reef Remote Sensing: A Guide for Mapping, Monitoring and Management*, Springer, Dordrecht, Germany, pp. 79-112.

Hedley, J.D., Harborne, A.R., and Mumby, P.J. (2005), Simple and robust removal of sun glint for mapping shallow water benthos, *International Journal of Remote Sensing*, Vol. 26, No. 10, pp. 2107-2112.

Jensen, J. R. (2005), *Introductory Digital Image Processing:A Remote Sensing Perspective, 3rd Edition*, Prentice Hall, Upper Saddle River, N.J.

Kim, H. (2014), *Extraction of Geospatial Information of Coastal Area Using Airborne Hyperspectral Imagery and LiDAR DEM*, Ph.D. dissertation, Kumoh National Institute of Technology, Gumi, Korea, 123p.

Kim, T., Choi, Y., Choi, J., Kwon, M., and Park, H. (2013), Comparison between in situ survey and satellite imagery with regard to coastal habitat distribution patterns in Weno, Micronesia, *Ocean and Polar Research*, Vol. 35, No. 4, pp. 395-405.

Lyzenga, D. R. (1978), Passive remote sensing techniques for

mapping water depth and bottom features, *Applied Optics*, Vol. 17, No. 3, pp. 379-383.

Mishra, D.R., Narumalani, S., Rundquist, D., Lawson, M., and Perk, R. (2007), Enhancing the detection and classification of coral reef and associated benthic habitats: A hyperspectral remote sensing approach, *Journal of Geophysical Research*, Vol. 112, No. C8.

NOAA Coastal Services Center (2010), *Lake Michigan Basin Land Cover Change Report*, Report, NOAA Coastal Services Center, USA, pp. 1-13.

Oh, Y., Kim, B., Park, B., Choi, Y., and Nam, S. (2004), A study on the seabed information of the Korean coast, *Proceedings of the Korean Association of Geographic Information Studies Conference*, Korea Spatial Information Society, 1 March, Seoul, Korea, pp. 273-278.

Pittman, S.J., Costa, B., and Wedding, L.M. (2013), LiDAR applications, In: Goodman, J.A., Purkis, S.J., and Phinn, S.R. (eds.), *Coral Reef Remote Sensing: A Guide for Mapping, Monitoring and Management*, Springer, Dordrecht, Germany, pp. 145-174.

Seo, D. and Kim, J. (2008), Extraction of water depth in coastal area using EO-1 Hyperion imagery, The Journal of *The Korean Institute of Maritime Information and Communication Sciences*, Vol. 12, No. 4, pp. 716-723.

Shafri, H.Z.M., Suhaili, A., and Mansor, S. (2007), The performance of maximum likelihood, spectral angle mapper, neural network and decision tree classifiers in hyperspectral image analysis, *Journal of Computer Science*, Vol. 3, No. 6, pp. 419-423.

Tamir, C. and Arnon, K. (2015), Ground-level classification of a coral reef using a hyperspectral camera, *Remote Sensing*, Vol. 7, No. 6, pp. 7521-7544.

Wozencraft, J.M. and Park, J.Y. (2013), Integrated LiDAR and hyperspectral, In: Goodman, J. A., Purkis, S. J. and Phinn, S. R. (eds.), *Coral Reef Remote Sensing: A Guide for Mapping, Monitoring and Management*, Springer, Dordrecht, Germany, pp. 175-191.

Yang, C., Goolsby, J. A., Everitt, J. H., and Du, Q. (2012), Applying six classifiers to airborne hyperspectral imagery for detecting giant reed, *Geocarto International*, Vol. 27, No. 5, pp. 413-424.

Zavalas, R., Ierodiaconou, D., Ryan, D., Rattray, A., and Monk, J. (2014), Habitat classification of temperate marine macroalgal communities using bathymetric LiDAR, *Remote Sensing*, Vol. 6, No. 3, pp. 2154-2175.